Chemical Engineering Journal 164 (2010) 246–254

Contents lists available at ScienceDirect

Chemical Engineering Journal

journal homepage: www.elsevier.com/locate/cej

Modeling of a solid oxide electrolysis cell for carbon dioxide electrolysis

Meng Ni *

Department of Building and Real Estate, The Hong Kong Polytechnic University, Hung Hom, Kowloon, Hong Kong, China

ARTICLE INFO

Article history:
Received 10 December 2009
Received in revised form 3 July 2010
Accepted 16 August 2010

Keywords:
Solid oxide electrolyte
Transport phenomena
Porous media
Solid oxide fuel cell (SOFC)
Computational fluid dynamics (CFD)
Finite volume method (FVM)

ABSTRACT

In this study, two models are developed to investigate the performance of a solid oxide electrolysis cell (SOEC) for CO_2 electrolysis at different levels. The first model is a one-dimensional model which is basing on a previously developed electrochemical model for steam electrolysis and considered all overpotentials in the SOEC. The second model is a two-dimensional thermal-fluid model consisting of the 1D model and a computational fluid dynamics (CFD) model. It is found that the mean electrolyte temperature initially decreases with increasing operating potential, reaches the minimum at about 1.1 V and increases considerably with a further increase in potential. At the thermal-neutral voltage (1.463 V at 1173 K), the calculated mean electrolyte temperature matches the inlet gas temperature. Increasing the operating potential increases both the local current density and the electrolyte Nernst potential. The electrochemical performance can be improved by increasing the inlet gas velocity from 0.2 m s^{-1} to 1.0 m s^{-1} but further increasing the inlet gas velocity will not considerably enhance the SOEC performance. It is also found that a change of electrode permeability in the order of 10^{-16} m^2 to 10^{-13} m^2 does not noticeably influence the SOEC performance in the present study, due to negligible convection effect in the porous electrodes.

1. Introduction

Because of its good ionic conductivity at high temperatures (873–1273 K), yttria-stabilized zirconia (YSZ) has been widely used as an electrolyte material in solid oxide fuel cells (SOFCs) for electricity generation and solid oxide electrolysis cells (SOECs) for H_2 generation through steam electrolysis [1–8]. In addition to steam electrolysis, SOECs can also be used for CO_2 electrolysis to generate O_2 [9]. In recent years, NASA has initiated a few projects to study the CO_2 electrolysis for O_2 generation by an SOEC with platinum or nickel cermet electrodes [9–11]. In addition, a few other groups also started their research on CO_2 electrolysis [12].

Since most of the research works on CO_2 electrolysis are experimental in nature, the present literature is lacking detailed mathematical modeling of CO_2 electrolysis. Although there are some valuable modeling studies on steam electrolysis for H_2 production using SOECs [5–8], a pertinent modeling or reliable analysis on CO_2 electrolysis is needed to understand the physical–chemical processes in an SOEC used for CO_2 electrolysis. Chan et al. [13] developed an electrolyte model for CO_2 electrolysis, however, the important gas transport phenomenon in porous electrodes was not considered. In this study, two models are developed for CO_2 electrolysis by an SOEC at different levels. The 1D model is basing on a previously developed electrochemical model for steam electrolysis and considers all irreversible losses, including ohmic, activation and concentration overpotentials. The second model is a 2D thermal-fluid model where the heat and mass transfer as well as electrochemical reactions in the SOEC are all modeled. The models presented in this paper are different from the previously published models, as the Nernst potential and all the source terms in 2D model for carbon dioxide electrolysis are different from SOFCs or steam electrolysis. For example, fuel cell reaction is exothermic while carbon dioxide electrolysis is endothermic in nature. According to the author's knowledge, this is the first comprehensive modeling study on carbon dioxide electrolysis for oxygen production. Parametric simulations are performed to understand the coupled transport and electrochemical reactions in an SOEC used for CO_2 electrolysis. The effects of inlet gas velocity, electrode permeability and inlet gas composition on SOEC performance are investigated. The thermal-neutral voltage of SOEC for carbon dioxide electrolysis is discussed.

2. Model development

2.1. Operating mechanisms

The fundamental working mechanisms and a 2D view of an SOEC for CO_2 electrolysis are illustrated in Figs. 1 and 2, respectively. Similar to an SOFC, the SOEC used for CO_2 electrolysis consists of a porous cathode, a porous anode and a dense elec-

* Corresponding author. Tel.: +852 2766 4152; fax: +852 2764 5131.
E-mail addresses: memni@graduate.hku.hk, bsmengni@polyu.edu.hk.

1385-8947/$ – see front matter © 2010 Elsevier B.V. All rights reserved.
doi:10.1016/j.cej.2010.08.032

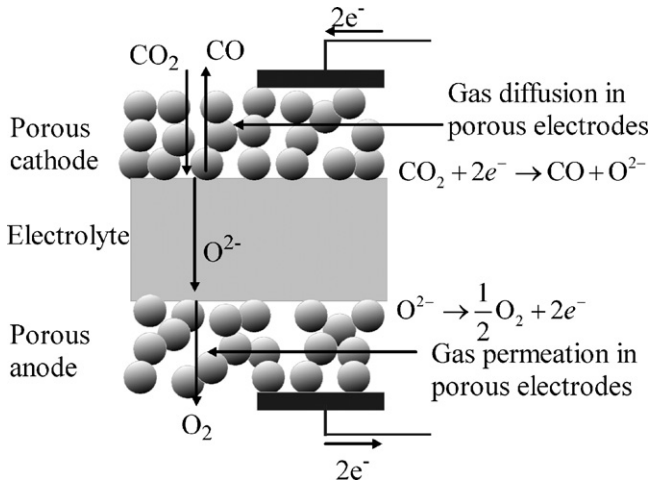

Fig. 1. Working mechanisms of CO_2 electrolysis by an SOEC.

trolyte. During operation, a sufficient electric potential is applied to the SOEC. CO_2 molecules are fed to the porous cathode and transported through the porous layer to the cathode-electrolyte interface, where they are reduced to CO and oxygen ions (O^{2-}). The generated CO molecules are transported out of the porous cathode and get collected, while the O^{2-} are transported through the dense electrolyte to the anode side. At the anode–electrolyte interface, oxygen ions are oxidized to form O_2 and electrons (e^-). The generated O_2 molecules are subsequently transported out of the porous anode while the electrons are transported to the cathode through the external circuit to complete the cycle. The net reaction of CO_2 electrolysis by an SOEC can be expressed as:

$$CO_2 \rightarrow CO + 0.5O_2 \tag{1}$$

2.2. One-dimensional electrochemical model of an SOEC used for CO_2 electrolysis

The required potential (V) applied to the SOEC can be written as:

$$V = E + \eta_{conc,c} + \eta_{conc,a} + \eta_{act,c} + \eta_{act,a} + \eta_{ohmic} \tag{2}$$

$$E = E_0 + \frac{RT}{2F} \ln \left[\frac{P^0_{CO} \left(P^0_{O_2}\right)^{0.5}}{P^0_{CO_2}} \right] \tag{3}$$

where E is the equilibrium voltage; E_0 is the equilibrium potential at standard pressure (about 0.924 V at 1200 K); F is the Faraday constant (96,485 C mol^{-1}); R is the ideal gas constant (8.3145 J mol^{-1} K^{-1}); T is the operating temperature (K); P^0 is the partial pressure at the electrode surface; and the subscripts CO_2, CO, and O_2 represent the carbon dioxide reactant, carbon monoxide and oxygen products, respectively; $\eta_{conc,c}$ and $\eta_{conc,a}$ are the concentration overpotentials at the cathode and anode, respectively; η_{ohmic} is the ohmic overpotential; and $\eta_{act,c}$ and $\eta_{act,a}$ are the activation overpotentials at the cathode and anode, respectively.

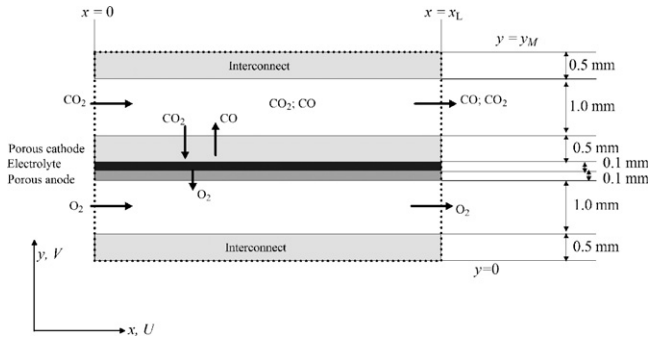

Fig. 2. 2D view of a planar SOEC used for CO_2 electrolysis.

At a temperature between 800 K and 1200 K, the equilibrium potential E_0 can be approximately calculated by a linear formula as,

$$E_0 = 1.1043 - 0.00045\,(T - 800) \tag{4}$$

The ohmic and activation overpotentials can be determined with the Ohm's law and Butler–Volmer equation, respectively. It should be mentioned that the Butler–Volmer equation may not be the best formula for describing the activation overpotential of SOEC electrodes, as for many good SOEC/SOFC composite electrodes, their current density–voltage relationships are usually rather linear. Nevertheless, Butler–Volmer equation is used in the current study and can be easily modified in the future if more experimental data are available to support a better formula for activation overpotential. Since the materials used for CO_2 electrolysis can be the same with those for H_2O electrolysis, the electrolyte (YSZ) conductivity and electrode exchange current density for steam electrolysis [14] are used for CO_2 electrolysis in the present study. However, the parameters should be updated if reliable data for CO_2 electrolysis are available.

In a previous study on SOEC used for steam electrolysis, the concentration overpotentials at the electrodes have been derived and analytical solutions have been obtained [15]. By substituting H_2O and H_2 with CO_2 and CO, respectively, the analytical solution of the cathode concentration overpotential ($\eta_{conc,c}$) of an SOEC used for CO_2 electrolysis can be obtained [15],

$$\eta_{conc,c} = \frac{RT}{2F} \ln \left[\frac{P^0_{CO_2}[P^0_{CO} + (RTJd_c/2FD^{eff}_{CO_2})]}{P^0_{CO}[P^0_{CO_2} - (RTJd_c/2FD^{eff}_{CO_2})]} \right] = \frac{RT}{2F} \ln \left[\frac{1 + (RTJd_c/2FD^{eff}_{CO_2}P^0_{CO})}{1 - (RTJd_c/2FD^{eff}_{CO_2}P^0_{CO_2})} \right] \tag{5}$$

where J is the current density (A/m^2), d_c is the thickness of the cathode (m), and $D^{eff}_{CO_2}$ is the effective diffusion coefficient (m^2/s) of CO_2, which can be obtained using the Bosanquet formula

$$\frac{1}{D^{eff}_{CO_2}} = \frac{\xi}{\varepsilon} \left(\frac{1}{D_{CO_2-CO}} + \frac{1}{D_{CO_2,k}} \right) \tag{6}$$

where ξ/ε is the ratio of electrode tortuosity to porosity; D_{CO_2-CO} is the molecular diffusion coefficient for CO_2–CO binary system; and $D_{CO_2,k}$ is the Knudsen diffusion coefficient of CO_2.

The molecular diffusion coefficient (D_{CO_2-CO}) and the Knudsen diffusion coefficient ($D_{CO_2,k}$) can be calculated as [16,17],

$$D_{CO_2-CO} = \frac{0.0026T^{1.5}}{PM^{0.5}_{CO_2-CO}\sigma^2_{CO_2-CO}\Omega_D} \tag{7}$$

$$D_{CO_2,k} = \frac{2r}{3}\sqrt{\frac{8RT}{\pi M_{CO_2}}} \tag{8}$$

$$M_{CO,CO_2} = \frac{2}{(1/M_{CO}) + (1/M_{CO_2})} \tag{9}$$

where M_{CO_2} and M_{CO} are the molecular weight of CO_2 and CO; r is the mean pore radius; σ_{CO_2-CO} is the mean characteristic length of species CO_2 and CO; and Ω_D is a dimensionless diffusion collision

Table 1
Parameters used in calculating the effective diffusion coefficients.

	CO	CO_2
σ_i	3.69	3.941
ε_i/k	91.7	195.2

integral. σ_{CO_2-CO} and Ω_D can be calculated as [16],

$$\sigma_{CO_2-CO} = \frac{\sigma_{CO} + \sigma_{CO_2}}{2} \tag{10}$$

$$\Omega_D = \frac{1.06036}{\tau^{0.1561}} + \frac{0.193}{\exp(0.47635\tau)} + \frac{1.03587}{\exp(1.52996\tau)} + \frac{1.76474}{3.89411\tau} \tag{11}$$

where the values of σ_{CO_2} and σ_{CO} can be found from Table 1 (ref. [16]). τ is the dimensionless temperature of CO_2 and CO binary system and can be calculated as,

$$\tau = \frac{k_b T}{\varepsilon_{i,j}} \tag{12}$$

where $k_b = 1.38066 \times 10^{-23}\ (J/K)$ is the Boltzmann's constant.

At the anode, oxygen is the only gas transporting in the porous electrode. Darcy's law can be used to describe the mass transport of O_2 in the anode. The analytical solution of anode concentration overpotential ($\eta_{conc,a}$) has been obtained in a previous study as [15],

$$\eta_{conc,a} = \frac{RT}{4F} \ln\left(\frac{\sqrt{(JRT\mu d_a/2FB_g) + \left(P^0_{O_2}\right)^2}}{P^0_{O_2}} \right) \tag{13}$$

where B_g is the permeability (m^2) of the porous anode and can be determined with the Kozeny–Carman relationship [18]; μ is the dynamic viscosity (kg/(m s)) of O_2, which can be obtained from reference [17]; and d_a is the thickness of the porous anode.

2.3. Two-dimensional thermal-fluid model of a planar SOEC used for CO_2 electrolysis

The 1D electrochemical model is useful for quick estimation of the current density-voltage of SOEC. However, in practice, the temperature, gas composition and current density are all varied along the gas channel. In order to obtained detailed information inside the SOEC, a 2D thermal-fluid model is needed.

2.3.1. Governing equations

The 2D thermal-fluid model is developed to study the coupled heat/mass transport and electrochemical reaction in a planar SOEC used for CO_2 electrolysis. The transport phenomena in an SOEC can be described in the general form as [19],

$$\frac{\partial(\rho\phi)}{\partial t} + \nabla(\rho V\phi) = \nabla(\Gamma\nabla\phi) + S \tag{14}$$

where ϕ is a general variable to be solved, t is time, ρ is density, V is the velocity vector, Γ is the general diffusion coefficient, and S is the general source term. By setting $\phi = 1$, the above general transport equation is reduced to the continuity equation. Replacing ϕ with U and V, Eq. (14) becomes momentum equations in x and y directions, respectively. By setting $\phi = Y_j$, the mass fraction of species j, the general transport equation (Eq. (14)) becomes the species equations. Substituting ϕ with temperature T, the general transport equation can be transformed to the energy equation. As a summary, the governing equations for conservation of mass, momentum, energy and species are written below,

$$\frac{\partial(\rho U)}{\partial x} + \frac{\partial(\rho V)}{\partial y} = S_m \tag{15}$$

$$\frac{\partial(\rho UU)}{\partial x} + \frac{\partial(\rho VU)}{\partial y} = -\frac{\partial P}{\partial x} + \frac{\partial}{\partial x}\left(\mu\frac{\partial U}{\partial x}\right) + \frac{\partial}{\partial y}\left(\mu\frac{\partial U}{\partial y}\right) + S_x \tag{16}$$

$$\frac{\partial(\rho UV)}{\partial x} + \frac{\partial(\rho VV)}{\partial y} = -\frac{\partial P}{\partial y} + \frac{\partial}{\partial x}\left(\mu\frac{\partial V}{\partial x}\right) + \frac{\partial}{\partial y}\left(\mu\frac{\partial V}{\partial y}\right) + S_y \tag{17}$$

$$\frac{\partial(\rho c_P UT)}{\partial x} + \frac{\partial(\rho c_P VT)}{\partial y} = \frac{\partial}{\partial x}\left(k\frac{\partial T}{\partial x}\right) + \frac{\partial}{\partial y}\left(k\frac{\partial T}{\partial y}\right) + S_T \tag{18}$$

$$\frac{\partial(\rho UY_i)}{\partial x} + \frac{\partial(\rho VY_i)}{\partial y} = \frac{\partial}{\partial x}\left(\rho D_{i,m}\frac{\partial Y_i}{\partial x}\right) + \frac{\partial}{\partial y}\left(\rho D_{i,m}\frac{\partial Y_i}{\partial y}\right) + S_{sp} \tag{19}$$

The density of the mixture ρ is calculated as

$$\rho = \frac{1}{\sum_{i=1}^{N} Y_i/\rho_i} \tag{20}$$

where Y_i and ρ_i are the mass fraction and density of species i.

The mass fraction and molar fraction of species i are related by

$$Y_i = X_i\left(\frac{M_i}{M}\right) \tag{21}$$

and

$$M = \sum_{i=1}^{N} X_i M_i \tag{22}$$

The effective heat capacity (c_p) and thermal conductivity (k) can be calculated as,

$$c_p = \varepsilon c_{p,f} + (1-\varepsilon)c_{p,s} \tag{23}$$

$$k = \varepsilon k_f + (1-\varepsilon)k_s \tag{24}$$

where k_f and k_s are the heat conductivity (W/(m K)) of the fluid and solid, respectively; $c_{p,f}$ and $c_{p,s}$ are the heat capacity (J/(kg K)) of the fluid and solid, respectively.

The source terms in continuity equation (Eq. (15)) and species equation (Eq. (19)) represent the change in mass and specie's mass fraction due to the electrochemical reactions at the active surface (electrode–electrolyte interface). At the cathode–electrolyte interface, the source term for continuity equation can be calculated as,

$$S_m = \left(\frac{JM_{CO}}{2F} - \frac{JM_{CO_2}}{2F}\right)\frac{A_{active}}{V_c} \tag{25}$$

where A_{active} is the area of active surface and V_c is the control volume. The ratio of V_c to A_{active} is the width (in y direction, Δy) of the control volume at the electrode–electrolyte interface. At the anode–electrolyte interface, the source term for continuity equation is calculated as,

$$S_m = \frac{JM_{O_2}}{4F}\frac{A_{active}}{V_c} \tag{26}$$

The source terms in momentum equations (Eqs. (16) and (17)) enable the momentum equations to be valid for both the gas channels and the porous electrodes and can be determined with the Darcy's law (Eqs. (27) and (28)).

$$S_x = \frac{\mu U}{B_g} \tag{27}$$

Table 2
Entropy (S, J/(K mol)) of O_2, CO and CO_2 [20].

Temperature (K)	O_2	CO	CO_2
800	235.921	227.277	257.494
900	239.931	231.074	263.645
1000	243.578	234.538	269.299
1100	246.922	237.726	274.528
1200	250.010	240.679	279.390

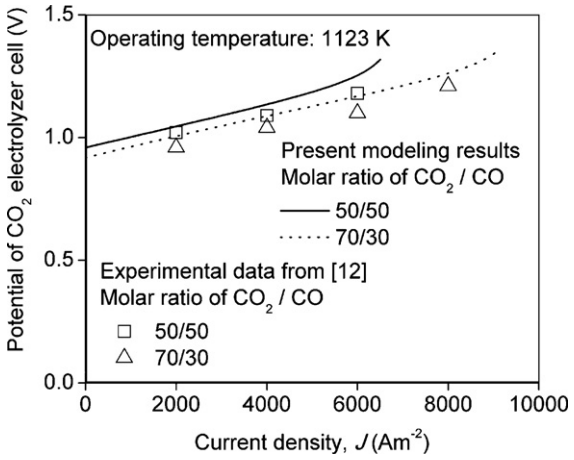

Fig. 3. Comparison of simulation results with experimental data [12] for model validation.

Table 3
Parameters used in 1D electrochemical modeling analysis of an SOEC for CO_2 electrolysis [14,16,23].

Parameter	Value
Operating temperature, T (K)	1,073
Operating pressure, P (bar)	1.0
Electrode porosity, ε	0.4
Electrode tortuosity, ξ	5.0
Average pore radius, r_p (μm)	0.5
Electrolyte conductivity (Ω^{-1} m^{-1})	$3.34 \times 10^4 \exp(-10300/T)$
Exchange current density (A/m^2)	
Cathode	5300
Anode	2000
Anode-supported SOEC	
Anode thickness d_a (μm)	500
Electrolyte thickness, L (μm)	50
Cathode thickness, d_c (μm)	50

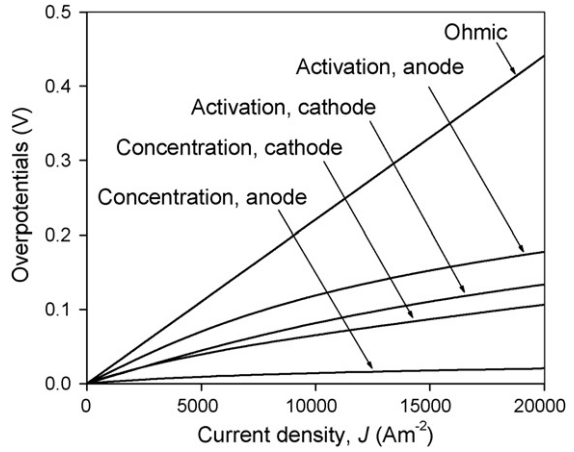

Fig. 4. Theoretical activation, concentration, and ohmic overpotentials of an anode-supported SOEC.

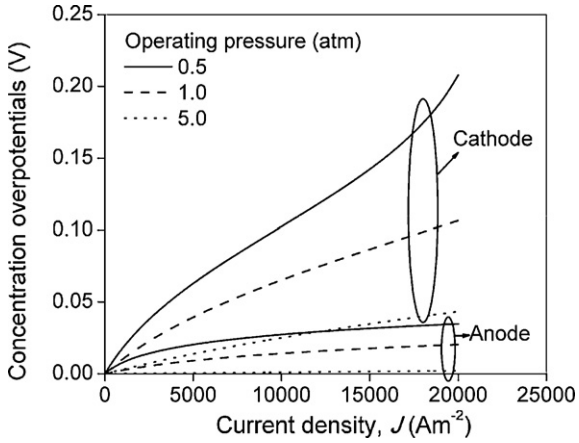

Fig. 5. Effect of operating pressure on concentration overpotentials.

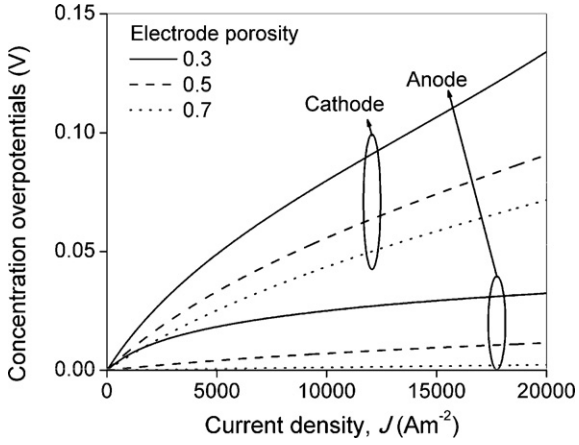

Fig. 6. Effect of electrode porosity on concentration overpotentials.

$$S_y = \frac{\mu V}{B_g} \tag{28}$$

The source term in the energy equation (Eq. (18)) results from the (1) heating effect by overpotential losses, including the ohmic, activation and concentration overpotentials and (2) entropy change of the electrochemical reaction. The source term can be calculated

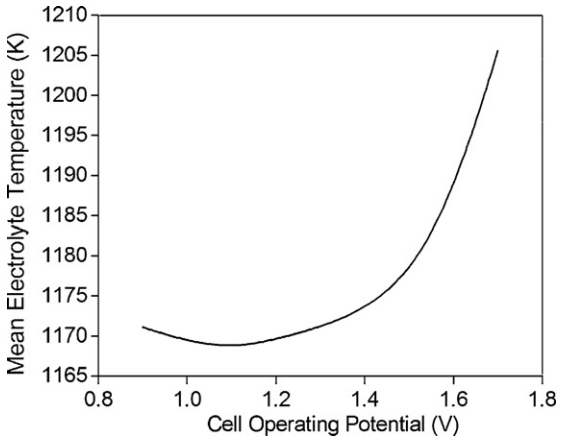

Fig. 7. Mean electrolyte temperature versus operating potential. (a) Effect of operating potential on current density distribution. (b) Effect of operating potential on electrolyte Nernst potential distribution.

Table 4
Parameters used in 2D thermal-fluid modeling analysis of a planar SOEC for CO_2 electrolysis [22].

Parameter	Value
Operating temperature, T (K)	1173
Operating pressure, P (bar)	1.0
Electrode porosity, ε	0.4
Electrode tortuosity, ξ	3.0
Average pore radius, r_p (μm)	0.5
Cathode-supported planar SOEC	
Cathode thickness d_c (μm)	500
Electrolyte thickness, L (μm)	100
Anode thickness, d_a (μm)	100
Height of gas flow channel (mm)	1.0
Length of the planar SOEC (mm)	20
Thickness of interconnect (mm)	0.5
Inlet velocity: U_{in} (m s^{-1})	0.5
SOEC operating potential (V)	1.3
Thermal conductivity of SOEC component (W m^{-1} K^{-1})	
Cathode	11.0
Electrolyte	2.7
Anode	6.0
Interconnect	1.1

as,

$$S_T = \left(-\frac{JT\Delta S}{2F} + J\eta_t\right)\frac{A_{active}}{V_c} \quad (29)$$

where η_t (V) is the total overpotential losses, which can be calculated as,

$$\eta_t = \eta_{conc,c} + \eta_{conc,a} + \eta_{act,c} + \eta_{act,a} + \eta_{ohmic} = V - E \quad (30)$$

The entropy change (ΔS, J/(K mol)) for the carbon dioxide electrolysis can be calculated as,

$$\Delta S = 0.5S_{O_2} + S_{CO} - S_{CO_2} \quad (31)$$

where S_{O_2}, S_{CO} and S_{CO_2} are entropy of O_2, CO, and CO_2, respectively, which can be found in Table 2 [20].

2.3.2. Numerical methodology

The governing equations presented above are discretized into algebraic equations by using the finite volume method (FVM) on a staggered grid arrangement [21]. The details of the numerical method and the boundary conditions can be found in the literature [22]. The source terms in the governing equations are related to the local current density, which is computed based on the updated gas composition and temperature for a given terminal cell potential. Computation is repeated till convergence is obtained. The in-house computational fluid dynamic (CFD) code was written and developed in FORTRAN.

3. Results and discussion

3.1. Model evaluation

In literature, only Mogensen's group [12] reported the detailed J–V characteristics and operating/structural parameters of CO_2 electrolysis by an SOEC for O_2 generation. Therefore, their data are used for model evaluation. In their experiments, the J–V data of a cathode-supported SOEC were measured. The cathode, electrolyte,

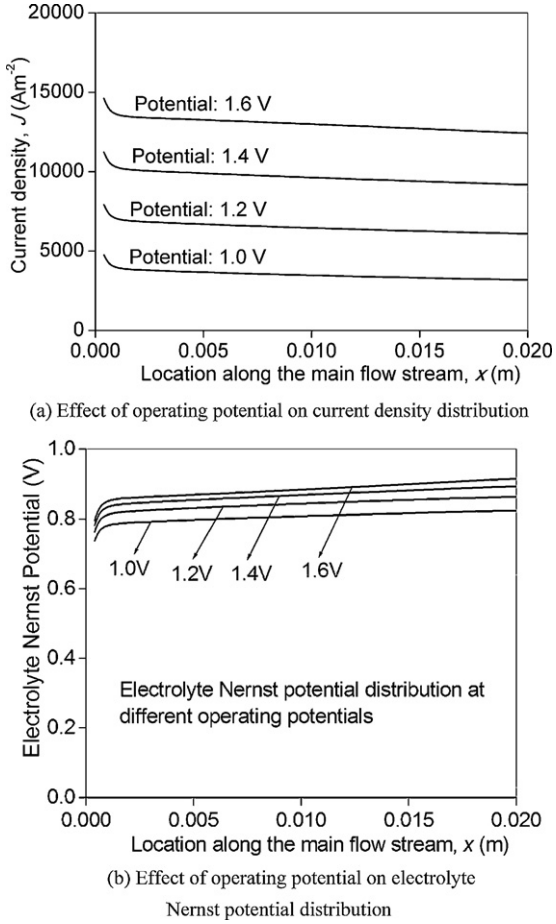

(a) Effect of operating potential on current density distribution

(b) Effect of operating potential on electrolyte Nernst potential distribution

Fig. 8. Effect of operating potential on SOEC performance. (a) Operating potential: 1.0 V. (b) Operating potential: 1.6 V.

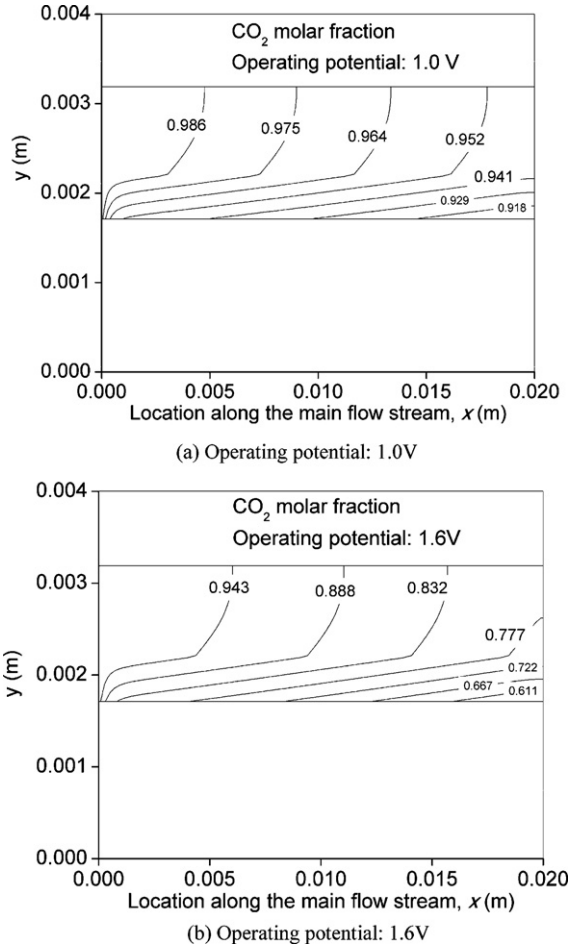

(a) Operating potential: 1.0V

(b) Operating potential: 1.6V

Fig. 9. Effect of operating potential on CO_2 molar fraction distribution at the cathode. (a) Operating potential: 1.0 V. (b) Operating potential: 1.6 V.

and anode were made of Ni/YSZ, YSZ, and LSM-YSZ (YSZ is yttria-stabilized zirconia) with thicknesses of about 312.5 μm, 12.5 μm, and 17.5 μm, respectively. Measurements were performed at an ambient pressure, a temperature of 1123 K, and various molar ratios of CO_2/CO (70/30 and 50/50). As shown in Fig. 3, the simulation results agree reasonably well with the experimental data from literature [12], thus validate the 1D electrochemical model developed in this paper. The validation of the 2D thermo-fluid model has been reported elsewhere [22] and is not repeated here.

3.2. Parametric simulations using the 1D electrochemical model

The typical parameters used for SOFC are used for SOEC simulation and are summarized in Table 3 [14,16,23].

3.2.1. Overpotentials of an SOEC

To understand the electrochemical characteristics of an SOEC, individual overpotentials of an anode-supported SOEC for CO_2 electrolysis are studied and shown in Fig. 4. Despite its thin thickness, the ohmic overpotential dominates the total overpotential. Activation overpotentials are also important electrical energy losses in CO_2 electrolysis. This is because the thermodynamic stability of CO_2 makes the electrolysis of CO_2 sluggish and CO_2 electrolysis involves complicated processes, such as gas adsorption/desorption and charge transfer. Although the concentration overpotentials are lower than the ohmic and activation overpotentials, their effect on SOEC performance should be carefully studied, as they can be high and can limit the SOEC performance under certain conditions.

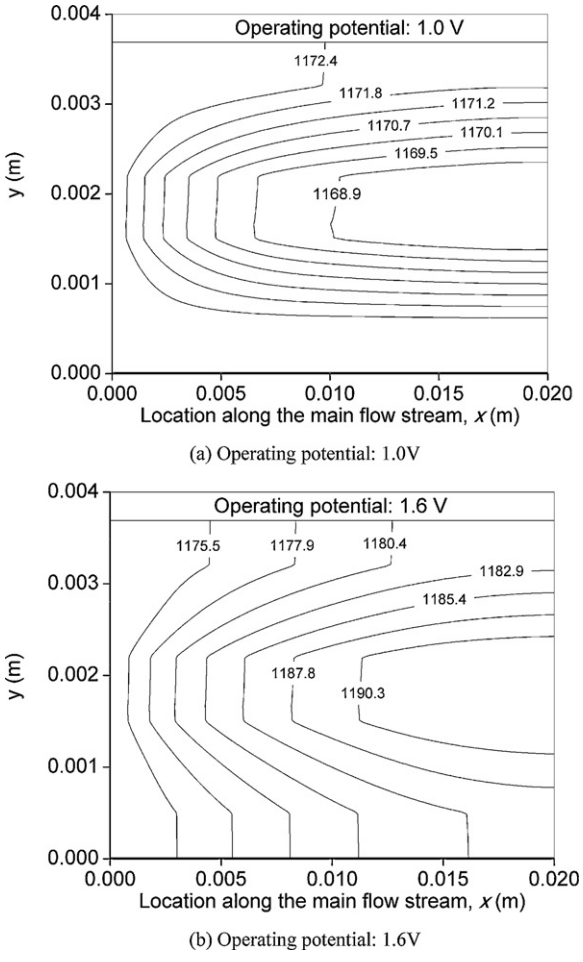

Fig. 10. Effect of operating potential on temperature distribution. (a) Current density distribution. (b) Electrolyte Nernst potential distribution.

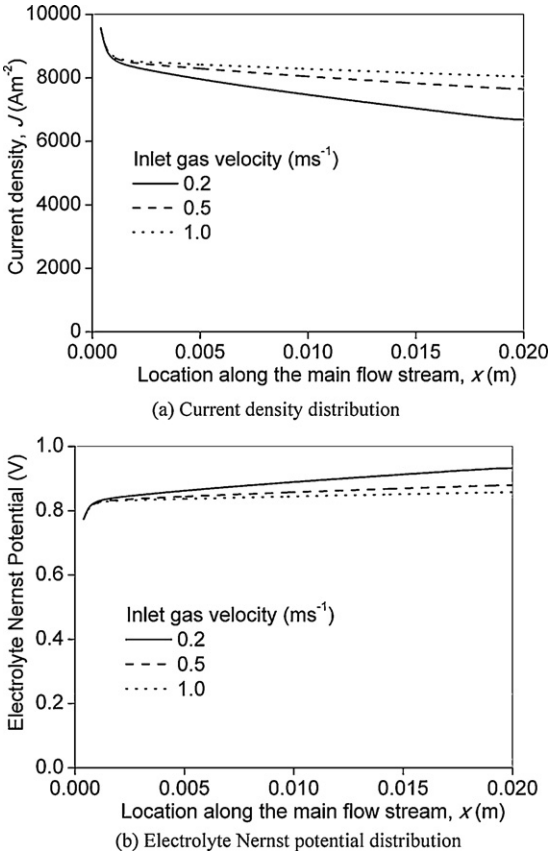

Fig. 11. Effect of inlet gas velocity on SOEC performance. (a) Inlet gas velocity: 0.2 m s^{-1}. (b) Inlet gas velocity: 0.5 m s^{-1}. (c) Inlet gas velocity: 1.0 m s^{-1}.

Among all overpotential losses, the concentration overpotential at the oxygen electrode (anode in SOEC mode) is the smallest. It is smaller than 0.02 V even at very high current density (20,000 A/m^2), due to very small resistance of the porous electrode to the permeation process of oxygen.

3.2.2. Operating and structural parameters on SOEC performance

The effect of operating pressure on SOEC potential is shown in Fig. 5. As can be seen from Eqs. (6)–(8), the binary diffusion coefficient (D_{CO_2-CO}) is inversely proportional to the operating pressure (P), but the Knudsen diffusion coefficient ($D_{CO_2,k}$) is independent of P, thus, the effective diffusion coefficient ($D^{eff}_{CO_2}$) is less sensitive to P. On the other hand, the gas density significantly increases with increasing pressure. The combined effects result in an increase in molar diffusion rate and a decrease in concentration overpotential with increasing pressure (Fig. 5).

The effect of electrode porosity on the concentration overpotentials of an SOEC is presented in Fig. 6. It is found that the concentration overpotentials at the cathode and anode decrease with increasing electrode porosity. The effective diffusion coefficient is proportional to the electrode porosity, as a high porosity implies that more space in the porous electrodes is available for gas diffusion. Therefore, a high electrode porosity is desired to improve the electric performance of an SOEC for CO_2 electrolysis. However, it should be mentioned that the activation overpotentials are assumed to be independent of the electrode microstructures, which is valid for conventional SOEC electrodes and might be invalid for advanced composite electrodes [24,25]. In order to account for the electrode structural effect on activation overpotentials, micro-scale modeling is needed.

3.3. Results of 2D thermal-fluid model

The typical parameters for planar SOFCs are used for 2D thermal-fluid modeling of SOECs for CO_2 electrolysis and are summarized in Table 4 [22]. Simulations are conducted to understand the coupled transport and electrochemical reactions in the SOEC.

3.3.1. Discussion on the thermal-neutral voltage (TNV) of SOEC

In CO_2 electrolysis, the CO_2 reduction reaction is endothermic, while the overpotential losses during operation generate ohmic heating. As the endothermic heat sink increases linearly while the ohmic heating increases rapidly with increasing current density, the net heat generation is negative at low current densities, increases to zero at a current density corresponding to the thermal-neutral voltage (TNV), and positive at higher current densities.

Fig. 7 shows the calculated mean electrolyte temperature as a function of operating potential. At a temperature of 1173 K, the TNV for CO_2 electrolysis is calculated to be about 1.463 V, with the method developed by Hawkes et al. [26]. Theoretically, the endothermic heat sink and the ohmic heat generation should be balanced at the TNV and the mean electrolyte temperature should be the same as the inlet gas temperature. In the present study, it is found that the mean electrolyte temperature is 1173.1 K at TNV (1.463 V), which is very close to the temperature at the gas inlet (1173.0 K).

3.3.2. Operating potential effect

The effects of operating potential on current density and Nernst potential are shown in Fig. 8. As expected, the current density increases with increasing operating potential and decreases along the main flow stream, as shown in Fig. 8(a). The decrease in current density is due to the increase in electrolyte Nernst potential along the gas flow channels (Fig. 8(b)). Along the gas flow channel, the molar ratio of CO/CO_2 increases (Fig. 9), raising the Nernst potential (Fig. 8(b)) and thus decreasing the current density (Fig. 8(a)). The change in current density and Nernst potential is significant

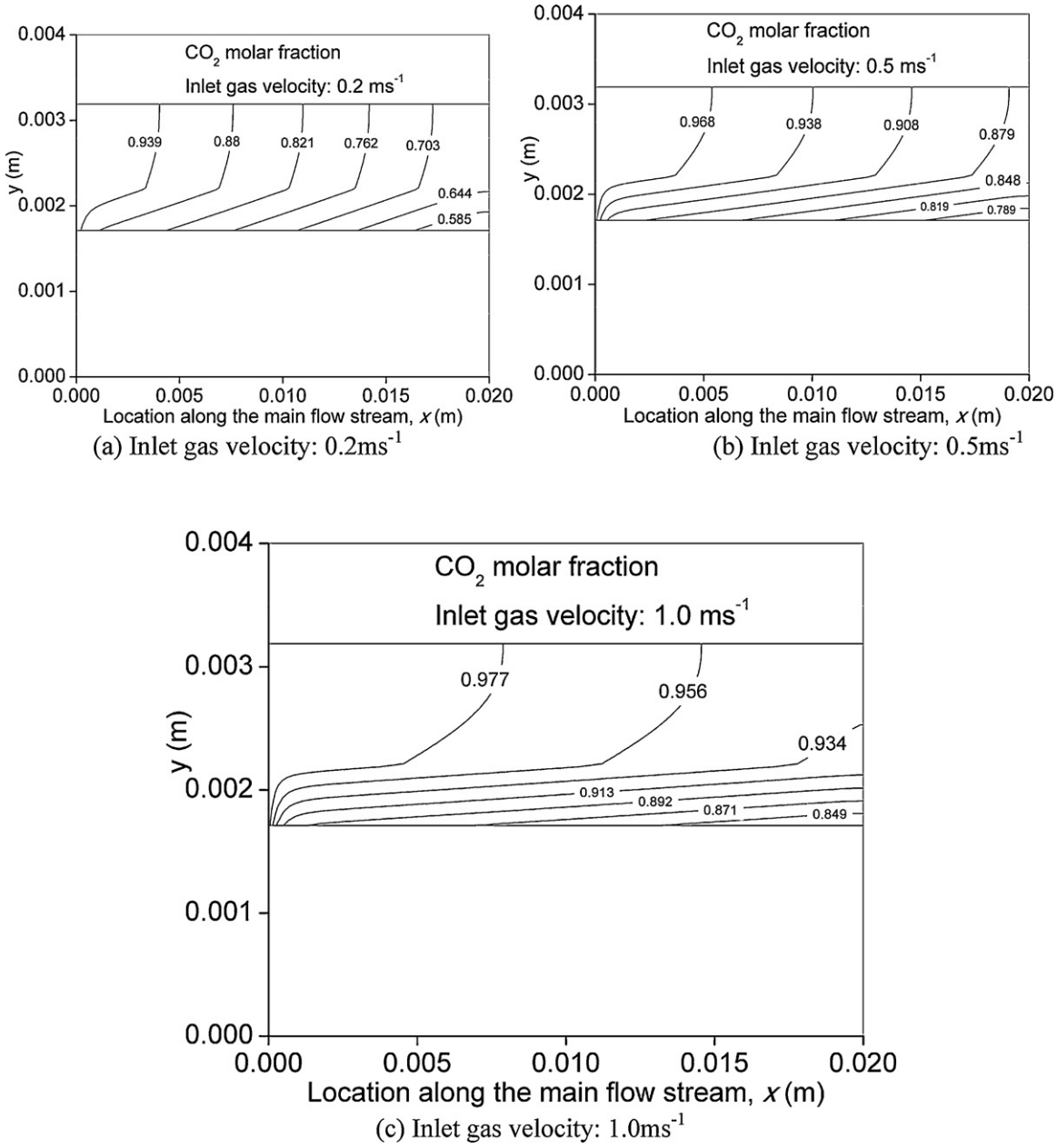

Fig. 12. Effect of inlet gas velocity on CO_2 molar fraction distribution at the cathode. (a) Current density distribution. (b) Electrolyte Nernst potential distribution.

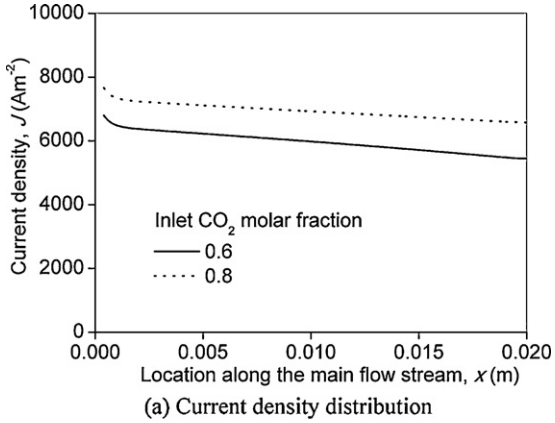

(a) Current density distribution

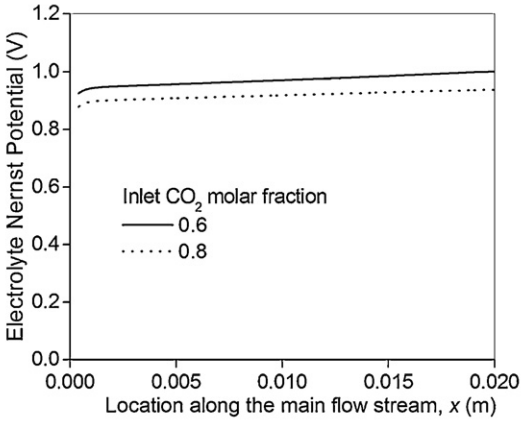

(b) Electrolyte Nernst potential distribution

Fig. 13. Effect of inlet CO_2 molar fraction on SOEC performance.

near the inlet because of the boundary conditions, since the gas velocity at the inlet of the porous electrode ($x = 0$) is zero. It is also found that the gradient of gas composition in the porous electrode is higher than in the gas channel, indicating the resistance of porous structure to gas diffusion in the electrode. At a higher operating potential, the change in molar ratio of CO/CO_2 is more significant (Fig. 9(a) and (b)), due to a higher current density (electrochemical reaction rate).

Fig. 10(a) and (b) shows the temperature contours of the SOEC at operating potentials of 1.0 V and 1.6 V, respectively. As discussed above, the SOEC temperature decreases along the gas flow channel at an operating potential of 1.0, as it is smaller than the TNV (1.463 V). At an operating potential of 1.6 V, the SOEC temperature increases along the gas channel, as the ohmic heat generation is higher than the heat requirement for the electrochemical reaction. At the same longitudinal location (x), considerable temperature gradients in the y direction are found for the gas streams. For comparison, the temperature gradient in y direction is small in the solid part, due to high thermal conductivity of the solid structures.

3.3.3. Effects of operating parameters – inlet gas velocity and gas composition

Fig. 11(a) and (b) shows the effect of inlet gas velocity on distributions of current densities and Nernst potentials. At the inlet, both the local current density and Nernst potential do not vary with inlet gas velocity, as the gas composition and temperature are the same at the inlet. At the downstream, the local current density increases and Nernst potential decrease with increasing inlet gas velocity. This is because at a higher inlet gas velocity, the gas composition along the main flow stream is more uniform than at a

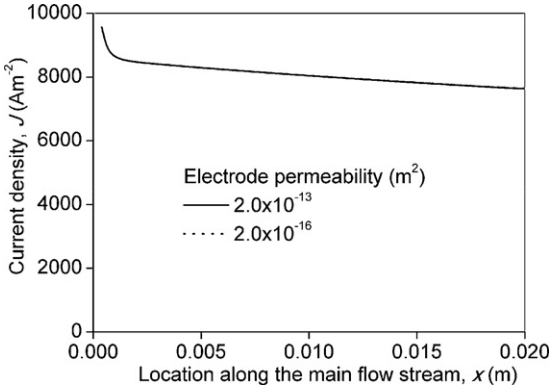

Fig. 14. Effect of electrode permeability on current density distribution.

lower inlet gas velocity (Fig. 12(a)–(c)), which in turn decreases the electrolyte Nernst potential and increases the local current density. For example, the average current density is increased from 7505 A m^{-2} at an inlet gas velocity of 0.2 m s^{-1} to 8300 A m^{-2} at an inlet gas velocity of 1.0 m s^{-1}. Since the differences in current density and Nernst potential between 0.5 m s^{-1} and 1.0 m s^{-1} are small, it is expected that further increase in inlet gas velocity will not significantly improve the SOEC performance.

The effect of inlet gas composition on SOEC performance is shown in Fig. 13(a) and (b). With a decrease in inlet CO_2 molar fraction, the local current density decreases and electrolyte Nernst potential increases. This phenomenon can be explained easily by the formula of the Nernst potential (Eq. (3)). In order to save electric power for CO_2 electrolysis, high CO_2 molar fraction is needed.

3.3.4. Effect of electrode permeability

In literature, the values of SOFC electrode permeability vary from 10^{-16} m^2 to 10^{-13} m^2 [27], it is therefore meaningful to examine whether the use of different values of electrode permeability can greatly affect the SOEC performance. Fig. 14 shows the local current density distributions in SOECs with different values of electrode permeability. It is found that increasing the electrode permeability from 10^{-16} m^2 to 10^{-13} m^2 almost does not influence the current density distribution. In the porous electrodes of an SOEC, the transport of gas species is mainly by means of diffusion and permeation is generally negligible. Since the diffusion process is independent of the electrode permeability, changing the electrode permeability in the studied range (10^{-16} m^2 to 10^{-13} m^2) does not significantly influence the SOEC performance.

4. Conclusions

Two models of increasing complexity are developed to study SOECs for CO_2 electrolysis at different levels. The first model is a 1D model extended from a previously developed electrochemical model for steam electrolysis, which considers all important electrochemical losses including ohmic, activation and concentration overpotentials. The second model is a 2D model integrating the 1D model and a 2D thermal-fluid model. Detailed heat and mass transfer in both the gas channels and the porous electrodes are fully considered in the 2D model.

Through electrochemical modeling analysis, it is found that the ohmic overpotential of the electrolyte dominates the total overpotential and activation overpotentials are also significant due to sluggish CO_2 electrolysis rate. Compared with the anode, the cathode concentration overpotential is more significant as the large molecular weights of CO_2 and CO result in small effective diffusion coefficients of CO_2 and CO. The cathode concentration overpotential can be considerably reduced by increasing the operating

pressure or increasing the electrode porosity. However, it should be mentioned that the current study does not consider the electrode structural effect on activation overpotential thus micro-scale modeling is needed in designing optimal electrode structures.

Parametric simulations are conducted using the 2D model to investigate the coupled transport and electrochemical reactions in a planar SOEC. At an operating potential lower than the TNV (1.463 V at 1173 K), the mean electrolyte temperature decreases with increasing potential, reaches the minimum at a potential about 1.1 V and then increases with further increase in operating potential. At the TNV, the calculated mean electrolyte temperature matches very well the inlet gas temperature, indicating that the heat requirement for electrochemical reduction of CO_2 is balanced by the ohmic heat generation. An increase in operating potential considerably increases the local current density, which in turn leads to lower CO_2 molar fraction and higher Nernst potential. Increasing the inlet gas velocity increases the SOEC electric performance due to more uniform distribution of gas composition along the flow channel. In addition, the local current density can be enhanced by increasing the inlet CO_2 molar fraction, due to reduced Nernst potential. It is also found that varying the electrode permeability in the range of 10^{-16} m^2 to 10^{-13} m^2 does not noticeably influence the SOEC performance.

The models developed in this paper are capable of predicting the SOEC performance at 1D and 2D levels. In order to better understand the physical–chemical processes, 3D models will be developed in the future. In addition, energy and exergy analysis will be conducted in the future to optimize the overall efficiency of the SOEC system.

References

[1] W. Jamsak, S. Assabumrungrat, P.L. Douglas, N. Laosiripojana, R. Suwanwarangkul, S. Charojrochkul, E. Croiset, Performance of ethanol-fuelled solid oxide fuel cells: proton and oxygen ion conductors, Chemical Engineering Journal 133 (1–3) (2007) 187–194.

[2] P. Piroonlerkgul, W. Wiyaratn, A. Soottitantawat, W. Kiatkittipong, A. Arpornwichanop, N. Laosiripojana, S. Assabumrugrat, Operation viability and performance of solid oxide fuel cell fuelled by different feeds, Chemical Engineering Journal 155 (1–2) (2009) 411–418.

[3] Z. Gao, Z.Q. Mao, C. Wang, J.B. Huang, Z.X. Liu, Composite electrolyte based on nano-structured $Ce_{0.8}Sm_{0.2}O_{1.9}$(SDC) for low-temperature solid oxide fuel cells, International Journal of Energy Research 33 (13) (2009) 1138–1144.

[4] Z.Q. Mao, Fuel Cells, Chemical Industry Press, Beijing, 2005.

[5] G.L. Hawkes, J. O'Brien, C. Stoots, B. Hawkes, 3D CFD model of a multi-cell high-temperature electrolysis stack, International Journal of Hydrogen Energy 34 (2009) 4189–4197.

[6] J.S. Herring, J.E. O'Brien, C.M. Stoots, G.L. Hawkes, J.J. Hartigsen, M. Shahnam, Progress in high-temperature electrolysis for hydrogen production using planar SOFC technology, International Journal of Hydrogen Energy 32 (2007) 440–450.

[7] J. Udagawa, P. Aguiar, N.P. Brandon, Hydrogen production through steam electrolysis: model-based steady-state performance of a cathode-supported intermediate temperature solid oxide electrolysis cell, Journal of Power Sources 166 (2007) 127–136.

[8] J. Udagawa, P. Aguiar, N.P. Brandon, Hydrogen production through steam electrolysis: model-based dynamic behavior of a cathode-supported intermediate temperature solid oxide electrolysis cell, Journal of Power Sources 180 (2008) 46–55.

[9] G. Tao, K.R. Sridhar, C.L. Chan, Study of carbon dioxide electrolysis at electrode/electrolyte interface: part I. Pt/YSZ interface, Solid State Ionics 175 (2004) 615–619.

[10] G. Tao, K.R. Sridhar, C.L. Chan, Study of carbon dioxide electrolysis at electrode/electrolyte interface: part II. Pt-YSZ cermet/YSZ interface, Solid State Ionics 175 (2004) 621–624.

[11] K.R. Sridhar, B.T. Vaniman, Oxygen production on Mars using solid oxide electrolysis, Solid State Ionics 93 (1997) 321–328.

[12] S. Dalgaard Ebbesen, M. Mogensen, Electrolysis of carbon dioxide in solid oxide electrolysis cells, Journal of Power Sources 193 (2009) 349–358.

[13] S.H. Chan, X.J. Chen, K.A. Khor, An electrolyte model for ceramic oxygen generator and solid oxide fuel cell, Journal of Power Sources 111 (2002) 320–328.

[14] M. Ni, M.K.H. Leung, D.Y.C. Leung, An electrochemical model of a solid oxide steam electrolyzer for hydrogen production, Chemical Engineering & Technology 29 (2006) 636–642.

[15] M. Ni, M.K.H. Leung, D.Y.C. Leung, A modeling study on concentration overpotentials of a reversible solid oxide fuel cell, Journal of Power Sources 163 (2006) 460–466.

[16] E. Hernandez-Pacheco, D. Singh, P.N. Hutton, N. Patel, M.D. Mann, A macro-level model for determining the performance characteristics of solid oxide fuel cells, Journal of Power Sources 138 (2004) 174–186.

[17] R.C. Reid, J.M. Prausnitz, B.E. Poling, The Properties of Gases & Liquids, 4th Edition, McGraw-Hill Book Company, New York, 1987.

[18] J.H. Nam, D.H. Jeon, A comprehensive micro-scale model for transport and reaction in intermediate temperature solid oxide fuel cells, Electrochimica Acta 51 (2006) 3446–3460.

[19] C.Y. Wang, Fundamental models for fuel cell engineering, Chemical Reviews 104 (2004) 4727–4765.

[20] M.W. Chase, NIST-JANAF Thermochemical Tables, 4th ed., American Chemical Society, American Institute of Physics for the National Institute of Standards and Technology, 1998.

[21] S.V. Patankar, Numerical Heat Transfer and Fluid Flow, McGraw-Hill Book Company, New York, 1980.

[22] M. Ni, Modeling of a planar solid oxide fuel cell based on proton-conducting electrolyte, International Journal of Energy Research, in press, doi:10.1002/er.1620.

[23] S.H. Chan, K.A. Khor, Z.T. Xia, A complete polarization model of a solid oxide fuel cell and its sensitivity to the change of cell component thickness, Journal of Power Sources 93 (2001) 130–140.

[24] X.J. Chen, S.H. Chan, K.A. Khor, Simulation of a composite cathode in solid oxide fuel cells, Electrochimica Acta 49 (2004) 1851–1861.

[25] A. Ali, X. Wen, K. Nandakumar, J.L. Luo, K.T. Chuang, Geometrical modeling of microstructure of solid oxide fuel cell composite electrodes, Journal of Power Sources 185 (2008) 961–966.

[26] G.L. Hawkes, J.E. O'Brien, C.M. Stoots, J.S. Herring, CFD model of a planar solid oxide electrolysis cell for hydrogen production from Nuclear energy, The 11th International Topical Meeting on Nuclear Reactor Thermal-Hydraulics (NURETH-11), Avignon, France, 2–6 October 2005.

[27] E. Resch, Numerical and experimental characterization of convective transport in solid oxide fuel cells, MSc Thesis at Queen's University, Kingston, Ontario, Canada, 2008.